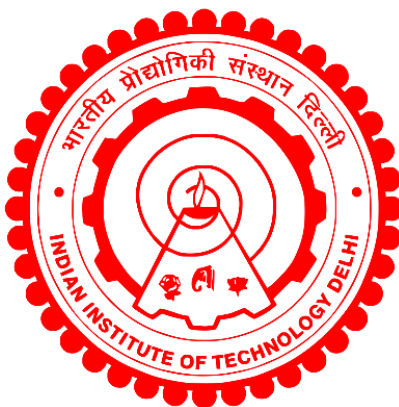


**BIODEGRADABLE POLYMERIC NANOPARTICLES
MEDIATED STIMULI-RESPONSIVE DELIVERY OF
CHEMOTHERAPEUTIC AGENTS FOR BREAST CANCER
THERAPY**

PRIYA GUPTA



**CENTRE FOR BIOMEDICAL ENGINEERING
INDIAN INSTITUTE OF TECHNOLOGY DELHI
SEPTEMBER 2025**

© Indian Institute of Technology Delhi (IITD), New Delhi, 2025

**BIODEGRADABLE POLYMERIC NANOPARTICLES
MEDIATED STIMULI-RESPONSIVE DELIVERY OF
CHEMOTHERAPEUTIC AGENTS FOR BREAST CANCER
THERAPY**

by

PRIYA GUPTA

Center for Biomedical Engineering

Submitted

**in the fulfilment of the requirements of the degree of Doctor of Philosophy
to the**



INDIAN INSTITUTE OF TECHNOLOGY DELHI

SEPTEMBER 2025

Dedicated to My Family...

CERTIFICATE

This is to certify that the thesis entitled “**BIODEGRADABLE POLYMERIC NANOPARTICLES MEDIATED STIMULI-RESPONSIVE DELIVERY OF CHEMOTHERAPEUTIC AGENTS FOR BREAST CANCER THERAPY**” submitted by **Ms. PRIYA GUPTA** to **Indian Institute of Technology Delhi** for the award of degree of Doctor of Philosophy in Biomedical Engineering is a record of bona fide research work carried out by her. **Ms. Priya Gupta** has worked under my supervision and has fulfilled the requirements for the submission of this thesis.

The results contained in this thesis are original and have not been submitted partially or fully to any other university or institute for the award of any degree or diploma.

Prof. Harpal Singh

Centre for Biomedical Engineering
Indian Institute of Technology Delhi
Hauz Khas, New Delhi – 110016

Prof. Ritu Kulshreshtha

Department of Biochemical Engineering and Biotechnology
Indian Institute of Technology Delhi
Hauz Khas, New Delhi – 110016

ACKNOWLEDGEMENTS

Pursuing a PhD has been a transformative journey—both intellectually and personally. It has shaped me into a more resilient, patient, and inquisitive individual. The challenges, uncertainties, and moments of self-doubt along the way taught me the value of perseverance, humility, and the importance of believing in the process. This journey has not only deepened my understanding of science but also enriched my perspective on life. I will always cherish this experience and the many lessons it brought along.

First and foremost, I would like to express my deep and sincere gratitude to my thesis supervisor, **Prof. Harpal Singh**, for his constant guidance, support and encouragement throughout the course of my PhD. His mentorship has been instrumental in shaping my research journey. Working under his supervision in his lab at IIT Delhi has been a truly enriching, productive and motivational experience. I deeply appreciate his tireless enthusiasm and insightful advice, which have greatly contributed to the completion of this work.

I gratefully acknowledge the financial assistance provided by the CSIR-JRF, which made this research possible. I would also like to sincerely thank my co-supervisor, **Prof. Ritu Kulshreshtha**, for her invaluable support, thoughtful suggestions and consistent encouragement. Her insightful discussions have always challenged me to think critically and improve as a researcher.

My heartfelt thanks to **Dr. Sandeep Kumar Jha**, **Dr. Jayanta Bhattacharya** and **Dr. Leena Nebhani**, for serving as members of my SRC committee. Their constructive feedback and inquisitive questions inspired me to broaden my perspective and deepen my understanding of the subject matter.

I extend my sincere gratitude to the administrative and instrumentation lab staff for their support in various official and technical matters throughout my PhD. I am especially thankful to **Mr. Rajesh Parasher** for his constant motivation and to **Mr. Anil Pandey** for his assistance with animal experiments. I am also deeply thankful to **Dr. Ankushi Bansal**, whose encouragement, guidance and support during challenging

times have left a lasting impact on me and her presence was a true pillar of strength in this journey.

It is a pleasure to acknowledge all my lab mates, whose contributions and companionship have greatly enriched this experience. The sense of friendship and teamwork within the lab created a supportive and inspiring environment. I am especially grateful to **Dr. Sachchidanand Tiwari** and **Dr. Anees Mohammad**, who served as my mentors and guided me through various aspects of research, be it experimental design, scientific writing, or ideation. Their mentorship, support and motivational conversations will always stay with me.

A special mention to **Harshdeep** - thank you for being the go-to person in tough situations. Your quiet strength and dependable nature made a world of difference. I would also like to acknowledge my senior lab members - **Dr. Neha Mehrotra**, **Mr. Manjeet Singh** and **Dr. Sruti Chattopadhyay** for their guidance and kindness and my juniors **Manleen**, **Sovan**, **Doyel**, **Shivani**, **Maneesha**, **Ali** and **Debatri** for their affection and support.

I am also thankful to **Dr. Yashveer Singh**, my previous mentor and to **Dr. Neelam Chauhan**, **Dr. Piyush Kumar** and **Dr. Moumita Halder** from my MSc dissertation lab at IIT Ropar, for sparking my early interest in research.

I am incredibly grateful to my friends at IIT Delhi, who made this phase of life vibrant and memorable. Special thanks to **Shruti**, **Vidit**, **Vaishali**, **Rachna**, **Kriti**, **Madhur**, **Mohit** and **Drishti** for being the reason IIT felt like a second home. I am deeply grateful to my close friends **Chitra**, **Rajat** and **Diksha** for their emotional support, genuine care and constant encouragement as your friendship has been a blessing. My family has been my greatest source of strength. I owe everything to the love and blessings of my parents, who raised me with strong values and gave me the freedom to chase my dreams. To my siblings, **Ankit** and **Pragati**, thank you for always standing by my side, listening patiently and offering unwavering support. Our bond, filled with countless fights and infinite love, means the world to me. I also want to

extend my gratitude to my **in-laws** for creating a welcoming and supportive environment that allowed me to pursue my academic aspirations.

And finally, the most special acknowledgment goes to my life partner, **Mr. Rishabh Murarka** - thank you for being my constant source of strength, peace and joy. Your unconditional support, patience and love were the foundation that helped me through this challenging journey. This milestone is as much yours as it is mine.

Lastly, I thank the **Almighty** for granting me the strength, opportunities and resilience to achieve this prestigious degree. I feel truly fortunate and humbled by this entire experience. Finally, I would like to express my sincere gratitude to all those who contributed to the successful completion of this thesis. I apologize for not being able to acknowledge each individual by name, but your support and contributions are truly appreciated, which helped me reach this important milestone in my life.

PRIYA GUPTA

ABSTRACT

According to World Health Organization, cancer remains the second leading cause of mortality worldwide, accounting for approximately 10 million deaths in 2020. Among various cancer types, breast cancer has consistently been the most frequently diagnosed malignancy in women and a leading cause of female cancer related deaths, with an estimated 2.3 million new cases and 685,000 deaths reported globally in 2020. Conventional treatment strategies for solid breast tumors rely heavily on surgery, radiation therapy and chemotherapy. Among chemotherapeutic agents, anthracyclines, particularly Doxorubicin (Dox), have been widely employed due to their broad-spectrum anti-cancer activity. However, the clinical utility of Dox is significantly limited by its dose-dependent cardiotoxicity and multidrug resistance. Pirarubicin (Pira), a semi-synthetic analogue of Dox with a tetrahydropyranyl (THP) substitution at the 4-O position, has emerged as a promising alternative due to its enhanced cellular uptake, reduced cardiotoxicity and efficacy in Dox-resistant tumor models. Combination chemotherapy remains a cornerstone strategy for overcoming drug resistance and achieving synergistic therapeutic effects by attacking cancer cells via multiple mechanisms. However, challenges such as mismatched pharmacokinetics of individual drugs and increased systemic toxicity hinder its clinical effectiveness. Nanotechnology based drug delivery platforms offer a promising solution by enabling site-specific drug accumulation through the enhanced permeability and retention (EPR) effect. In this context, polymeric nanoparticles have gained particular attention due to their tunability, biodegradability and ability to respond to tumor-specific stimuli such as pH or redox conditions. In the first phase of this research, Pirarubicin and Gemcitabine (Gem), an FDA-approved antimetabolite with limited therapeutic efficacy due to rapid deamination and systemic toxicity, were conjugated to an amphiphilic block copolymer (mPEG-b-PLA) via a Schiff base linker (Levulinic acid) to formulate pH-sensitive dual-drug-loaded nanoparticles. The resulting polymeric nanoparticle system exhibited uniform size distribution, low

polydispersity and favourable biocompatibility profiles. *In-vitro* release studies demonstrated accelerated drug release in acidic environments, corresponding to the tumor microenvironment. Furthermore, cellular uptake assays revealed enhanced internalization, while cytotoxicity studies indicated a synergistic effect of the Pira-Gem combination in some breast cancer cell lines. However, two critical limitations were encountered (i) The nanoformulation exhibited low drug-loading efficiency, attributed to the limited number of available conjugation sites on the polymer backbone, thereby necessitating a higher polymer-to-drug ratio, which poses potential concerns regarding systemic safety (ii) The observed therapeutic synergy between the drug combination was inconsistent across different breast cancer cell lines, underscoring the need for broader validation to establish universal applicability. To overcome these issues, a second nanoparticle system was designed using polyethyleneimine (PEI), a branched polyamine polymer known for its high density of functional groups. Polyethyleneimine (PEI) was used to form Schiff base linkages with both Pirarubicin (Pira) and Salinomycin (Sal). Sal is an ionophore antibiotic known for its strong ability to target and eliminate cancer stem cells (CSCs), which are major drivers of tumor recurrence and resistance. It was strategically combined with Pirarubicin to achieve a more potent and synergistic anticancer response. The resulting PEI-Pira/Sal conjugates were encapsulated within mPEG-b-PLA to improve biocompatibility and systemic circulation. The dual-loaded nanoparticles achieved a significantly higher drug loading (~90%) compared to the initial system and maintained excellent colloidal stability while retaining a moderately negative surface charge. *In-vitro* studies confirmed the enhanced cytotoxicity, synergistic therapeutic effects and effective CSC inhibition by Pira–Sal co-loaded nanoparticles across various drug ratios (1:1, 3:1, 1:3) and multiple breast cancer cell lines. The Pira–Sal (3:1) co-loaded nanoparticles showed the highest synergy and was selected for *in-vivo* evaluation. In syngeneic EAC tumor-bearing Balb/c mice, these nanoparticles led to ~95% tumor regression after biweekly intravenous injections. However, the survival analysis showed signs of systemic toxicity, as

most mice in both the single and dual-loaded nanoparticles treatment groups did not survive until the end of the study. This was likely caused by the release of free polyethyleneimine (PEI) upon degradation of the nanoparticle matrix, which is known to be toxic in its unbound form. These findings prompted the exploration of a safer, yet equally effective, alternative strategy. In the final phase of this work, a folic acid (FA)-conjugated, redox-responsive block copolymer system [S-(PLA-b-PEG-CONH)]₂, was developed to achieve active targeting and controlled drug release. Folic acid was employed as a targeting ligand to exploit the overexpression of folate receptors on various breast cancer subtypes, enhancing cellular uptake and tumor-specific accumulation. The copolymer, [S-(PLA-b-PEG-CONH)]₂, was synthesized through a multistep process and characterized by ¹H NMR spectroscopy and gel permeation chromatography (GPC). The number average (M_n) and weight average molecular weights (M_w) were determined to be 27,726 g/mol and 38,386 g/mol, respectively, with a polydispersity index of 1.384. Dual-loaded nanoparticles incorporating Pira and Sal in varying ratios (1:1, 3:1, 1:3) were formulated using the FA-conjugated redox-responsive polymer. The nanoparticles demonstrated excellent physicochemical stability, enhanced drug loading and prominent biocompatibility under physiological conditions. *In-vitro* assays showed significant improvements in cellular uptake in both 2D monolayer cultures and 3D tumor spheroids. The redox-sensitive disulfide bonds facilitated drug release in glutathione-rich environments typical of tumor intracellular conditions, while maintaining drug integrity under normal physiological conditions. Cytotoxicity and proliferation inhibition studies indicated that the Pira/Sal dual-loaded nanoparticles were significantly more effective than either free drug or singly-loaded nanoparticles. Moreover, the combination index (CI) analysis revealed consistent synergy across all tested ratios and folate receptor-positive breast cancer cell lines. The Pira/Sal (3:1) formulation was again selected for *in-vivo* evaluation due to its superior *in-vitro* performance. *In-vivo* studies in EAC tumor-bearing mice involved biweekly tail vein injections for 3 weeks, followed by monitoring for 60 days. The FA-

conjugated redox-responsive nanoparticles achieved nearly complete tumor regression with no observable tumor recurrence during the study duration. Importantly, there was no significant body weight loss in treated mice and histopathological evaluation of major organs revealed no signs of notable toxicity. These findings confirmed the *in-vivo* safety and therapeutic effectiveness of the formulation, in clear contrast to the earlier PEI-based system, which exhibited prominent toxicity. In conclusion, this work presents a comprehensive comparison of multiple polymeric nanoparticle-based strategies for combination chemotherapy in breast cancer. FA-conjugated, redox-responsive polymeric nanoparticles co-loaded with Pirarubicin and Salinomycin not only resolved critical limitations of previous formulations such as low drug loading, systemic toxicity and variable therapeutic responses but also demonstrated exceptional *in-vivo* compatibility and anti-tumor efficacy. This dual-targeted nanoformulation emerges as a potent and safe candidate for breast cancer therapy, with potential for clinical translation. Future investigations will focus on validation in higher animal models and advancement toward clinical trials.

सारांश

विश्व स्वास्थ्य संगठन के अनुसार, कैंसर अब भी वैश्विक स्तर पर मृत्यु का दूसरा सबसे बड़ा कारण बना हुआ है, और वर्ष 2020 में लगभग 1 करोड़ लोगों की मृत्यु कैंसर के कारण हुई। विभिन्न प्रकार के कैंसर में स्तन कैंसर महिलाओं में सबसे अधिक निदान किया जाने वाला कैंसर है और महिला कैंसर-जनित मृत्यु का एक प्रमुख कारण है, जिसके वर्ष 2020 में लगभग 2.3 मिलियन नए मामले और 6.85 लाख मौतें दर्ज की गईं। ठोस स्तन ट्यूमर के पारंपरिक उपचार में शल्य चिकित्सा, विकिरण चिकित्सा और कीमोथेरेपी शामिल हैं। कीमोथेरेपी एजेंट्स में, विशेष रूप से एंथ्रासाइक्लिन्स जैसे डॉक्सोर्बिसिन (Dox) का उपयोग व्यापक रूप से हुआ है। हालांकि, Dox की खुराक-निर्भर हृदय विषाक्तता और बहु-दवा प्रतिरोध इसके नैदानिक उपयोग को सीमित कर देते हैं। डॉक्सोर्बिसिन का एक अर्ध-प्राकृतिक एनालॉग पिरारूबिसिन (Pira), 4-O पोजीशन पर टेट्राहाइड्रोपायनिल (THP) प्रतिस्थापन के कारण, बेहतर कोशिकीय अवशोषण, कम हृदय विषाक्तता और Dox-प्रतिरोधी ट्यूमर मॉडलों में प्रभावशीलता के कारण एक आशाजनक विकल्प बन कर उभरा है। संयोजन कीमोथेरेपी, कैंसर कोशिकाओं पर विभिन्न जैविक मार्गों के माध्यम से हमला कर, दवा प्रतिरोध को दूर करने और संयुक्त चिकित्सीय प्रभाव प्राप्त करने की एक प्रमुख रणनीति है। हालांकि, व्यक्तिगत दवाओं की असंगत फार्माकोकाइनेटिक्स और बढ़ी हुई प्रणालीगत विषाक्तता इसकी नैदानिक प्रभावशीलता को बाधित करते हैं। नैनोटेक्नोलॉजी आधारित ड्रग डिलीवरी प्लेटफॉर्म, ट्यूमर स्थल पर लक्षित दवा संचय को EPR (Enhanced Permeability and Retention) प्रभाव के माध्यम से संभव बना कर इस चुनौती का समाधान प्रदान करते हैं। इस संदर्भ में, पॉलीमर नैनोपार्टिकल्स अपनी अनुकूलनशीलता, बायोडिग्रेडेबिलिटी और ट्यूमर-विशिष्ट उत्तेजनाओं (जैसे pH या रेडॉक्स स्थितियाँ) के प्रति उत्तरदायी होने के कारण विशेष ध्यान आकर्षित करते हैं। इस शोध के पहले चरण में, पिरारूबिसिन और जेमसिटाबीन (Gem) — एक FDA अनुमोदित एंटीमेटाबोलाइट जिसे तीव्र डीअमीनेशन और प्रणालीगत विषाक्तता के कारण सीमित प्रभावशीलता मिलती है — को एक अम्फीफिलिक ब्लॉक कोपॉलीमर (mPEG-b-PLA) से लेवुलिनिक एसिड आधारित शिफ बेस लिंकर्स के माध्यम

से जोड़ा गया ताकि pH-संवेदनशील द्वैत्य-दवा-युक्त नैनोपार्टिकल्स तैयार किए जा सकें। ये नैनोकण समान आकार वितरण, कम पॉलीडिस्पर्सिटी और बेहतर बायोअनुकूलता दर्शाते हैं। इन विट्रो रिलीज़ अध्ययनों ने अम्लीय वातावरण (जैसे ट्यूमर माइक्रोइनवायरनमेंट) में तेजी से दवा रिलीज़ को दिखाया। सेलुलर अवशोषण परीक्षणों से यह स्पष्ट हुआ कि इन नैनोकणों का अंतर्ग्रहण अधिक था, और साइटोटॉक्सिसिटी अध्ययनों ने कुछ स्तन कैंसर सेल लाइनों में Pira-Gem संयोजन के सहयोगी प्रभाव को दर्शाया। हालांकि, दो महत्वपूर्ण सीमाएँ सामने आईं —

(i) नैनोफॉर्मूलेशन में सीमित संयोजन स्थलों के कारण कम दवा-लोडिंग क्षमता पाई गई, जिससे अधिक पॉलीमर-से-दवा अनुपात की आवश्यकता हुई, जिससे प्रणालीगत सुरक्षा पर प्रभाव पड़ा,

(ii) विभिन्न स्तन कैंसर सेल लाइनों और दवा अनुपातों में चिकित्सीय समन्वय में असंगति देखी गई, जिससे इसकी सार्वभौमिकता पर प्रश्नचिह्न लगा। इन समस्याओं से निपटने के लिए, दूसरे चरण में पॉलीइथाइलीनइमीन (PEI) आधारित नैनोपार्टिकल सिस्टम को डिजाइन किया गया, जो एक शाखित पॉलीअमाइन है और इसकी उच्च कार्यात्मक समूह घनता के लिए जाना जाता है। PEI को पिरारूबिसिन (Pira) और सैलिनोमाइसिन (Sal) — एक आयोनोफोर एंटीबायोटिक जो कैंसर स्टेम कोशिकाओं (CSCs) को लक्षित करने और समाप्त करने में सक्षम है — दोनों से शिफ बेस लिंकर्स के माध्यम से जोड़ा गया। सैलिनोमाइसिन को पिरारूबिसिन के साथ संयोजन में इस उद्देश्य से चुना गया कि मिलकर वे अधिक शक्तिशाली और सहयोगी कैंसर-रोधी प्रभाव उत्पन्न करें। इन PEI-आधारित यौगिकों को mPEG-b-PLA से लपेटा गया ताकि उनकी बायोअनुकूलता और रक्त में स्थायित्व में सुधार हो। इस प्रणाली ने पहले की तुलना में ~90% तक उच्च दवा-लोडिंग और उत्कृष्ट कोलॉइडल स्थिरता दिखाई। इन विट्रो अध्ययनों में विभिन्न अनुपातों (1:1, 3:1, 1:3) और विभिन्न स्तन कैंसर सेल लाइनों में Pira-Sal युक्त नैनोकणों ने प्रभावशाली साइटोटॉक्सिसिटी, सहयोगी प्रभाव और CSCs को दबाने की क्षमता प्रदर्शित की। इनमें से Pira-Sal (3:1) संयोजन सर्वश्रेष्ठ परिणाम देने वाला पाया गया और इसे इन विवो परीक्षण के लिए चुना गया। Balb/c माइस में EAC ट्यूमर मॉडल पर यह प्रणाली ~95% ट्यूमर प्रतिगमन तक पहुँची। हालांकि, पशुओं की उत्तरजीविता विश्लेषण में यह सामने

आया कि अधिकांश माइस अध्ययन की समाप्ति से पहले ही मर गए, संभवतः फ्री PEI के कारण हुई विषाक्तता की वजह से। इसने एक अधिक सुरक्षित और प्रभावशाली वैकल्पिक रणनीति की आवश्यकता को जन्म दिया। तीसरे और अंतिम चरण में, एक फोलिक एसिड (FA)-संयुग्मित रेडॉक्स-संवेदनशील ब्लॉक कोपॉलीमर सिस्टम विकसित किया गया, जिसका उद्देश्य सक्रिय लक्ष्यीकरण और नियंत्रित दवा रिलीज़ प्राप्त करना था। FA को एक लक्ष्यीकरण लिगैंड के रूप में उपयोग किया गया ताकि स्तन कैंसर उपप्रकारों में अधिक व्यक्त फोलेट रिसेप्टर्स का लाभ उठाया जा सके, जिससे कोशिकीय अवशोषण और ट्यूमर-विशिष्ट संचय को बढ़ावा मिले। बहु-चरणीय संश्लेषण प्रक्रिया द्वारा तैयार इस [S-(PLA-b-PEG-CONH)]₂ को ¹H NMR और GPC के माध्यम से विशेषता प्रदान की गई। इसका M_n और M_w क्रमशः 27,726 g/mol और 38,386 g/mol पाया गया, और polydispersity index 1.384 था, जो एक समान पॉलीमर वितरण को दर्शाता है। Pira और Sal को विभिन्न अनुपातों (1:1, 3:1, 1:3) में FA-युक्त रेडॉक्स-संवेदनशील पॉलीमर से लोड किया गया। नैनोकणों ने उत्कृष्ट स्थायित्व, बेहतर दवा लोडिंग और उत्कृष्ट जैव-अनुकूलता प्रदर्शित की। इन विट्रो अध्ययनों में 2D और 3D कैंसर मॉडल में बेहतर कोशिकीय अंतर्ग्रहण देखा गया। GSH-समृद्ध ट्यूमर वातावरण में मौजूद रेडॉक्स-संवेदनशील डिसल्फाइड बॉन्ड्स ने लक्षित दवा रिलीज़ सुनिश्चित की, जबकि सामान्य शारीरिक स्थितियों में दवा की स्थिरता बनी रही। साइटोटाक्सिसिटी और सेल प्रसार अवरोधन अध्ययनों में यह देखा गया कि यह द्वैत्य-दवा युक्त प्रणाली मुक्त दवाओं या एकल-दवा युक्त नैनोकणों की तुलना में कहीं अधिक प्रभावशाली थी। संयोजन सूचकांक विश्लेषण ने सभी अनुपातों और FA-रेसेप्टर पॉजिटिव स्तन कैंसर कोशिकाओं में लगातार सहयोगी प्रभाव दिखाया। श्रेष्ठ प्रदर्शन वाले Pira/Sal (3:1) फॉर्मूलेशन को इन विवो परीक्षण के लिए फिर से चुना गया। EAC ट्यूमर-बेयरिंग माइस में 3 सप्ताह तक बायवीकली इंजेक्शन के बाद 60 दिनों तक मॉनिटरिंग की गई। इस सिस्टम ने ट्यूमर के लगभग पूर्ण प्रतिगमन को सुनिश्चित किया और अध्ययन अवधि में कोई पुनरावृत्ति नहीं हुई। शरीर के वजन में कोई महत्वपूर्ण गिरावट नहीं देखी गई और अंगों की हिस्टोपैथोलॉजिकल जांच में कोई विषाक्तता नहीं पाई गई। इन परिणामों ने पहले के विषाक्त PEI आधारित सिस्टम की तुलना में इस प्रणाली की सुरक्षा और प्रभावशीलता

को प्रमाणित किया। निष्कर्षतः, यह कार्य स्तन कैंसर की संयोजन कीमोथेरेपी के लिए विभिन्न नैनोपार्टिकल आधारित रणनीतियों की एक समग्र तुलना प्रस्तुत करता है। FA-संयुग्मित, रेडॉक्स-संवेदनशील पॉलीमर नैनोकणों ने पिरारूबिसिन और सैलिनोमाइसिन के साथ मिलकर पूर्ववर्ती फॉर्मूलेशनों की सीमाओं — जैसे कम दवा लोडिंग, प्रणालीगत विषाक्तता और असंगत चिकित्सीय प्रतिक्रियाओं — को सफलतापूर्वक हल किया और असाधारण जैव-संगतता व ट्यूमररोधी प्रभावशीलता दिखाई। यह द्वैत्य लक्षित प्रणाली स्तन कैंसर उपचार के लिए एक शक्तिशाली और सुरक्षित उम्मीदवार के रूप में उभरती है, जिसके नैदानिक अनुवाद की प्रबल संभावनाएं हैं। भविष्य के अध्ययनों में इसे उच्च स्तरीय प्राणी मॉडल में सत्यापित करना और नैदानिक परीक्षण की दिशा में अग्रसर होना प्रस्तावित है।

TABLE OF CONTENTS

CERTIFICATE.....	i
ACKNOWLEDGEMENT.....	iii
ABSTRACT.....	vi
TABLE OF CONTENTS.....	xiv
LIST OF CONTENT.....	xv
LIST OF FIGURES.....	xxiii
LIST OF TABLES.....	xxxi
GLOSSARY OF SYMBOLS AND ABBREVIATIONS.....	xxxiii

LIST OF CONTENT

CHAPTER 1 – Introduction and Literature Review

1.1 Global Burden of Cancer.....	2
1.2 Biological Hallmarks of Cancer.....	3
1.3 Epidemiology of Breast Cancer.....	5
1.4 Risk Factors for Breast Cancer.....	5
1.5 Molecular Classification of Breast Cancer.....	6
1.6 Mechanisms of Breast Cancer Development.....	7
1.7 Tumor Microenvironment and Immune Evasion.....	7
1.8 Clinical Challenges and the Need for Continued Research.....	8
1.9 Types of Cancer Therapies.....	8
1.9.1 Local Therapies.....	9
1.9.1.1 Surgery.....	9
1.9.1.2 Radiation Therapy.....	10
1.9.2 Systemic Therapies.....	10
1.9.2.1 Hormone (Endocrine) Therapy.....	10
1.9.2.2 Targeted Therapy.....	11
1.9.2.3 Immunotherapy.....	12
1.9.2.4 Stem Cell Therapy.....	13
1.9.3 Chemotherapy.....	13
1.10 Overview of Chemotherapy for breast cancer.....	14
1.10.1 Antimetabolites.....	15
1.10.2 Mitotic Spindle Inhibitors.....	15

1.10.3 Topoisomerase Inhibitors.....	16
1.10.4 Alkylating Agents.....	17
1.11 Limitations of Chemotherapy.....	18
1.11.1 Poor Aqueous Solubility.....	19
1.11.2 Low Stability in Blood Circulation.....	20
1.11.3 Rapid Clearance from the Body.....	20
1.11.4 Low Bioavailability at the Tumor Site.....	20
1.11.5 Development of Multi-Drug Resistance (MDR).....	20
1.11.6 Cancer Relapse and Recurrence.....	21
1.11.7 High Off-Target Cytotoxicity.....	21
1.12 Nanoparticles-Based Drug Delivery -A promising approach to overcome limitations of chemotherapy.....	22
1.13 Smart Polymeric Nanoparticles.....	28
1.13.1 pH-Responsive Stimuli (Internal).....	28
1.13.2 Redox-Responsive Stimuli (Internal).....	29
1.13.3 Enzyme-Responsive Stimuli (Internal).....	30
1.13.4 Temperature-Responsive Stimuli (External or Internal).....	31
1.13.5 Light-Responsive Stimuli (External).....	32
1.13.6 Ultrasound-Responsive Stimuli (External).....	33
1.13.7 Magnetic-Responsive Stimuli (External).....	34
1.13.8 Electric Field-Responsive Stimuli (External).....	35
1.14 Rationale and Objective of the Research Work.....	37
1.15 References.....	40

CHAPTER 2 – Development of Pirarubicin/Gemcitabine-Conjugated PLA-Based Block Copolymeric Nanoparticles for Anti-Cancer Efficacy

2.1 Introduction.....	66
2.2 Materials and Methods.....	69
2.2.1 Materials.....	69
2.2.2 Synthesis of mPEG-b-PLA block copolymer.....	69
2.2.3 Attachment of Levulinic acid to mPEG-b-PLA.....	70
2.2.4 Conjugation of Pira/Gem to mPEG-b-PLA-LA	70
2.2.5 Characterization of Pira/Gem-mPEG-b-PLA-LA conjugates.....	71
2.2.6 Calculation of % Drug conjugation efficacy.....	71
2.2.7 Preparation and characterization of nanoparticles using Pira/Gem-mPEG-b-PLA-LA conjugate.....	72
2.2.8 Toxicity analysis of nanoparticles.....	73
2.2.9 <i>In-vitro</i> drug release study of Pira/Gem mPEG-b-PLA-LA nanoparticles.....	74
2.2.10 Cellular uptake studies.....	75
2.2.11 Cell migration inhibition assay.....	75
2.2.12 Apoptosis study.....	76
2.2.13 Cell proliferation inhibition assay.....	76
2.2.14 Combination index evaluation.....	77
2.2.15 Statistical analysis.....	77
2.3 Results and Discussion.....	78
2.3.1 Chracterization of mPEG-b-PLA and LA conjugation.....	78
2.3.2 Drug conjugation efficiency.....	82

2.3.3	Preparation and characterization of nanoparticles.....	82
2.3.4	Toxicity analysis of nanoparticles.....	83
2.3.5	In-vitro release of nanoparticles.....	85
2.3.6	Cellular uptake of nanoparticles.....	88
2.3.7	Cell migration inhibition assay.....	89
2.3.8	Apoptosis study.....	91
2.3.9	Cytotoxicity studies of nanoparticles.....	92
2.3.10	Combination index evaluation.....	96
2.4	Conclusion.....	101
2.5	References.....	104

CHAPTER 3 – Development of Pirarubicin/Salinomycin-Polyethyleneimine Conjugates and Their Delivery Using PLA-Based Block Copolymeric Nanoparticles

3.1	Introduction.....	109
3.2	Materials and Methods.....	111
3.2.1	Materials.....	111
3.2.2	Methods.....	111
3.2.2.1	Synthesis and characterization of mPEG-b-PLA block copolymer.....	111
3.2.2.2	Synthesis and characterization of PEI-Pira or PEI-Sal conjugates.....	112
3.2.2.3	Preparation of PEI-Pira/Sal loaded mPEG-b-PLA nanoparticles.....	112
3.2.2.4	Physiological characterization of PEI-Pira/Sal loaded mPEG-b-PLA nanoparticles....	113
3.2.2.5	Biocompatibility analysis of PEI in mPEG-b-PLA nanoparticles.....	114
3.2.2.6	Cellular internalization study.....	115

3.2.2.7	<i>In-vitro</i> drug release study.....	115
3.2.2.8	Evaluation of cell migration inhibition via scratch assay.....	116
3.2.2.9	Cytotoxicity evaluation on 2D breast cancer cells <i>in-vitro</i>	117
3.2.2.10	Analysis of combination index.....	118
3.2.2.11	Cytotoxicity evaluation on 3D mammospheres <i>in-vitro</i>	118
3.2.2.12	<i>In-vivo</i> tumor inhibition studies.....	118
3.2.2.13	<i>In-vivo</i> toxicity evaluation.....	119
3.2.2.14	Statistical analysis.....	124
3.3	Results and Discussion	120
3.3.1	Synthesis and characterization of mPEG-b-PLA block copolymer.....	120
3.3.2	Synthesis and characterization of PEI-Pira or PEI-Sal conjugates	121
3.3.3	Preparation and characterization of PEI-Pira/Sal loaded mPEG-b-PLA nanoparticles.....	121
3.3.4	Biocompatibility analysis of PEI in mPEG-b-PLA nanoparticles.....	126
3.3.5	Cellular internalization study.....	127
3.3.6	<i>In-vitro</i> drug release study.....	129
3.3.7	Evaluation of cell migration inhibition via scratch assay.....	131
3.3.8	Cytotoxicity evaluation on 2D cells and 3D mammospheres <i>in-vitro</i>	131
3.3.9	Analysis of combination index.....	134
3.3.10	Cytotoxicity evaluation on 3D mammospheres <i>in-vitro</i>	136
3.3.11	<i>In-vivo</i> tumor inhibition studies.....	136
3.3.12	<i>In-vivo</i> toxicity evaluation.....	139
3.4	Conclusion.....	142
3.5	References.....	145

CHAPTER 4 – Development of Folic Acid-Conjugated Pirarubicin/Salinomycin Dual-Encapsulated PLA-Based Redox-Responsive Block Copolymeric Nanoparticles

4.1	Introduction.....	153
4.2	Materials and Methods.....	157
4.2.1	Materials.....	157
4.2.2	Synthesis and characterization of FA-conjugated [S-(PLA-b-PEG-CONH)] ₂ block copolymer.....	157
4.2.2.1	Synthesis of (OH-PLA-S-S-PLA-OH)	157
4.2.2.2	End group modification of (OH-PLA-S-S-PLA-OH) with succinic anhydride.....	158
4.2.2.3	PEGylation of (HOOC-PLA-S-S-PLA-COOH).....	158
4.2.2.4	Conjugation of Folic acid to [S-(PLA-b-PEG-COOH)] ₂	159
4.2.3	Preparation of FA-conjugated [S-(PLA-b-PEG-CONH)] ₂ block copolymeric nanoparticles.....	160
4.2.4	Characterization of FA-conjugated Pira/Sal loaded [S-(PLA-b-PEG-CONH)] ₂ block copolymeric nanoparticles.....	161
4.2.5	Stability evaluation of FA-conjugated [S-(PLA-b-PEG-CONH)] ₂ polymeric nanoparticles.....	161
4.2.6	Biocompatibility assessment of FA-conjugated [S-(PLA-b-PEG-CONH)] ₂ polymeric nanoparticles.....	162
4.2.7	Drug release profile in-vitro.....	163
4.2.8	Cellular uptake in 2D adherent cells and 3D mammospheres.....	163
4.2.9	2D Cell proliferation inhibition studies of free drug Pira/Sal vs FA-conjugated Pira/Sal dual-loaded nanoparticles.....	164

4.2.10	<i>In-vitro</i> cytotoxicity on 3D mammospheres.....	165
4.2.11	Combination index & Synergy evaluation.....	166
4.2.12	<i>In-vivo</i> tumor regression, toxicity and survival studies.....	166
4.2.13	Statistical analysis.....	167
4.2	Results and Discussion.....	167
4.3.1	Characterization of FA-conjugated [S-(PLA-b-PEG-CONH)] ₂ polymer.....	167
4.3.2	Preparation and characterization of FA-conjugated [S-(PLA-b-PEG-CONH)] ₂ nanoparticles.....	173
4.3.3	Stability examination of FA-conjugated [S-(PLA-b-PEG-CONH)] ₂ block copolymeric nanoparticles.....	175
4.3.4	Biocompatibility assessment of FA-conjugated [S-(PLA-b-PEG-COOH)] ₂ block copolymeric nanoparticles.....	177
4.3.5	Drug release profile <i>in-vitro</i>	178
4.3.6	Cellular uptake study on 2D adherent cells and 3D mammospheres	179
4.3.7	2D Cell proliferation inhibition studies of FA-conjugated Pira/Sal single or dual-loaded nanoparticles.....	181
4.3.8	<i>In-vitro</i> cytotoxicity on 3D mammospheres.....	182
4.3.9	Combination index & Synergistic efficacy calculation.....	185
4.3.10	<i>In-vivo</i> tumor regression, toxicity and survival study.....	185
4.3.11	Histopathological analysis.....	188
4.4	Conclusion.....	192
4.5	References.....	194

CHAPTER 5 – Summary and Future Directions

4.6	Summary of the research work.....	199
4.7	Future scope and direction of the research work.....	204

LIST OF FIGURES

CHAPTER 1 – Introduction and Literature Review

Fig. 1.1 Progression of cancer in body at cellular level	4
Fig. 1.2 Classification of commonly used chemotherapeutics depending on their mechanism of action	19
Fig. 1.3 Circulation and biodistribution of drug-loaded nanoparticles in the bloodstream	24
Fig. 1.4 Classification of stimuli-responsive polymeric nanoparticles according to various triggering stimuli	36
Fig. 1.5 Schematic representation of the workflow of the thesis	39

CHAPTER 2 – Development of Pirarubicin/Gemcitabine-Conjugated PLA-Based Block Copolymeric Nanoparticles for Anti-Cancer Efficacy

Fig. 2.1 Schematic illustration of mechanism of action of Pira-Gem co-loaded mPEG-PLA-LA block copolymeric nanoparticles on cancer cell	68
Fig. 2.2 Schematic representation of synthesis of block copolymer mPEG-b-PLA, attachment of levulinic acid and subsequent conjugation of Pirarubicin/Gemcitabine to the block copolymer	79
Fig. 2.3 ¹ H NMR spectra of block copolymer mPEG-b-PLA and mPEG-b-PLA-LA	80
Fig. 2.4 FTIR spectra of block copolymer mPEG-b-PLA and mPEG-b-PLA-LA	80
Fig. 2.5 ¹ H NMR spectra of Pira-mPEG-b-PLA-LA conjugate vs mPEG-b-PLA	81
Fig. 2.6 ¹ H NMR spectra of Gem-mPEG-b-PLA-LA conjugate vs mPEG-b-PLA	81
Fig. 2.7 Physicochemical characterization of mPEG-b-PLA-LA nanoparticles loaded with Pira, Gem, and	

Pira-Gem (1:1) combination. (A) Hydrodynamic size measurements of blank and drug-loaded nanoparticles. (B) Zeta potential analysis indicating surface charge variations across formulations. (C) Transmission Electron Microscopy (TEM) images illustrating nanoparticle morphology. (D) Particle size distribution with corresponding average size and standard deviation for each formulation. 84

Fig. 2.8 FE-SEM image of Pira loaded mPEG-b-PLA-LA nanoparticles 85

Fig. 2.9 Biocompatibility assessment of mPEG-b-PLA-LA nanoparticles. (A) Cytocompatibility on NIH 3T3 and HEK 293T cells via MTT assay. (B) Hemocompatibility evaluation through hemolysis analysis. 86

Fig. 2.10 *In-vitro* release profile of Pira and Gem from single-loaded and dual-loaded Pira/Gem-mPEG-b-PLA-LA nanoparticles at (A) tumor microenvironmental conditions with pH 6.8 (B) serum conditions with 10% FBS at pH 7.4 (C) only physiological pH (7.4). (D) lysosomal pH (5.0). Data are presented as mean \pm SD (n = 3); p > 0.05 considered not significant (ns) 87

Fig. 2.11 Cellular uptake of Pira-loaded mPEG-b-PLA-LA nanoparticles in SUM-149 cells. (A) Confocal laser scanning microscopy (CLSM) images (60 \times magnification; scale bar: 50 μ m) comparing intracellular localization of free Pira and Pira-loaded nanoparticles after incubation. (B) Quantitative analysis of mean fluorescence intensity (MFI) in the nucleus and cytoplasm at 1 h and 4 h post-incubation. Data are shown as mean \pm SD; p > 0.05 indicates no significant difference (ns). 90

Fig. 2.12 Flow cytometric (FACS) analysis of Pira-mPEG-b-PLA-LA nanoparticles compared to free Pira in SUM-149 cells to support CLSM findings 91

Fig. 2.13 Anti-migratory effect of drug-loaded mPEG-b-PLA-LA nanoparticles in MDA-MB-468 cells. (A) CLSM images (20 \times magnification; scale bar: 200 μ m) from scratch assay showing wound closure before and after treatment with Pira-loaded, Gem-loaded, or Pira-Gem co-loaded nanoparticles versus saline control. (B) Quantitative analysis of % wound closure using ImageJ. Data are presented as mean \pm SD (n = 3); p > 0.05 indicates no significant difference (ns). 93

Fig. 2.14 Apoptosis analysis of drug-loaded mPEG-b-PLA-LA nanoparticles in SUM-149 cells. (A) Flow cytometry (FACS) plots showing apoptosis profiles using Annexin V-FITC/PI dual staining after treatment with Pira-loaded, Gem-loaded, and Pira-Gem co-loaded nanoparticles. Quadrants represent: Q1 (viable), Q2 (early apoptotic), Q3 (late apoptotic), and Q4 (necrotic) cell populations. (B) Quantitative comparison of % cell populations in each apoptotic and necrotic phase across treatments. Data are shown as mean \pm SD (n = 3). Statistical analysis was done using two-way ANOVA with Tukey's test. * and * indicate significance in Q1 and Q3; # and # indicate significance in Q2 and Q4, compared to the free Pira group. 94

Fig. 2.15 Cytotoxicity comparison of free drugs and drug-loaded mPEG-b-PLA-LA nanoparticles formulations in breast cancer cell lines. (A) IC₅₀ values of free Pirarubicin versus Pira-loaded nanoparticles. (B) IC₅₀ values of free Gemcitabine versus Gem-loaded nanoparticles. Cytotoxicity was assessed using the MTT assay across various breast cancer cell lines (n = 3); p > 0.05 indicates no significant difference (ns). 95

Fig. 2.16 Dose-dependent cytotoxic effects of free Pirarubicin (Pira), Gemcitabine (Gem) and their combination (Pira–Gem) on breast cancer cells assessed via MTT assay. Sigmoidal dose–response curves were generated using GraphPad Prism v9.0 to determine IC₅₀ values. Data represent mean \pm SD (n = 3) 97

Fig. 2.17 Dose-dependent cytotoxic effects of Pirarubicin (Pira)-loaded, Gemcitabine (Gem)-loaded and dual-loaded (Pira–Gem) nanoparticles on breast cancer cells evaluated using the MTT assay. Sigmoidal dose–response curves were generated in GraphPad Prism v9.0 for IC₅₀ determination. Results are presented as mean \pm SD (n = 3). 98

Fig. 2.18 Scatter plots of Combination Index (CI) versus fraction affected (Fa) for free Pirarubicin (Pira) and Gemcitabine (Gem) combinations at varying molar ratios (1:1, 3:1 and 1:3) across different breast cancer cell lines. CI values were calculated using CompuSyn software to evaluate the synergistic, additive, or antagonistic effects of the drug combinations. 99

Fig. 2.19 Scatter plots of Combination Index (CI) versus fraction affected (Fa) for Pira–Gem dual drug-

loaded nanoparticles at varying molar ratios (1:1, 3:1 and 1:3) in different breast cancer cell lines. CI values were calculated using CompuSyn software to assess the nature of drug interaction (synergistic, additive, or antagonistic) following nanoparticle-mediated co-delivery 100

CHAPTER 3 – Development of Pirarubicin/Salinomycin-Polyethyleneimine Conjugates and Their Delivery Using PLA-Based Block Copolymeric Nanoparticles

Fig. 3.1 ¹H NMR spectra of mPEG-b-PLA block copolymer in CDCl₃ 121

Fig. 3.2 Synthesis and characterization of PEI-Pira conjugate. (A) Schematic representation of the synthesis of the PEI-Pira conjugate. (B) Comparative ¹H NMR spectra of PEI-Pira conjugate in DMSO-d₆ and free Pirarubicin in CDCl₃. 122

Fig. 3.3 Synthesis and characterization of PEI-Sal conjugate. (A) Schematic representation of the synthesis of the PEI-Sal conjugate. (B) Comparative ¹H NMR spectra of the PEI-Sal conjugate and free Salinomycin in DMSO-d₆. 123

Fig. 3.4 Schematic illustration of preparation of PEI-Pira/Sal co-loaded mPEG-b-PLA nanoparticles 124

Fig. 3.5 Physicochemical characterization of mPEG-b-PLA nanoparticles (A) Hydrodynamic size variation (B) Zeta potential measurements of blank and drug-loaded nanoparticles (C) TEM images of (i) blank, (ii) PEI-Pira-loaded and (iii) PEI-Sal-loaded mPEG-b-PLA nanoparticles 125

Fig. 3.6 Evaluation of the cytocompatibility of free PEI, blank mPEG-b-PLA nanoparticles and PEI-loaded mPEG-b-PLA nanoparticles on (A) HEK 293T cells and (B) NIH-3T3 cells using the MTT assay. Data are shown as mean ± SD (n = 3); p > 0.05 indicates no significant difference (ns) 127

Fig. 3.7 Comparative analysis of hemolysis (%) induced by free PEI, blank nanoparticles and PEI-loaded

nanoparticles on mouse-derived RBCs. Data are shown as mean \pm SD (n = 3); p > 0.05 indicates no significant difference (ns) 128

Fig. 3.8 Cellular uptake and co-localization analysis of dual dye-loaded mPEG-b-PLA nanoparticles in SUM-149 cells. (A) CLSM images (40 \times magnification) displaying intracellular distribution of Rhodamine B and Coumarin 6-loaded nanoparticles. (B) Quantitative uptake analysis using flow cytometry. (C) FACS scatter plot illustrating co-localization of both dyes within cells. 130

Fig. 3.9 *In-vitro* drug release profiles of single- and dual-loaded PEI-Pira/Sal mPEG-b-PLA nanoparticles under different pH conditions, simulating physiological and tumor microenvironments 132

Fig. 3.10 Anti-migratory activity of PEI-Pira/Sal nanoparticles in breast cancer cells. (A) Scratch assay images depicting the inhibition of cell migration following treatment with single- and dual-drug-loaded PEI-Pira/Sal nanoparticles. (B) Quantitative comparison of wound gap closure (%) after 24 hrs of treatment. Data are expressed as mean \pm SD (n = 3); p > 0.05 indicates no significant difference (ns). 133

Fig. 3.11 Cytotoxicity evaluation of PEI-Pira/Sal mPEG-b-PLA nanoparticles in breast cancer cell lines (A) and (B) Comparison of IC₅₀ values between nanoparticle-loaded (PEI-Pira/Sal) and free drug (Pira/Sal) formulations following MTT assay (C) Dose-dependent cytotoxicity profiles of single and dual-drug-loaded nanoparticles (Pira:Sal ratios of 1:1, 3:1 and 1:3) after 72 hrs treatment across various breast cancer cell lines assessed by MTT assay 135

Fig. 3.12 Combination Index vs fraction affected scatter plots of PEI-Pira/Sal mPEG-b-PLA dual-loaded nanoparticles (in varying Pira-Sal ratios; 1:1, 3:1 and 1:3) on different breast cancer cell lines calculated via CompuSyn software 137

Fig. 3.13 Evaluation of cytotoxic effects of nanoparticle formulations in MCF-based 3D tumor spheroids. (A) Confocal microscopy images showing structural integrity of 3D mammospheres. (B) Quantitative analysis of cell viability (%) after 72 hrs of treatment, determined using the CCK-8 assay. (C) Dose-response curve depicting the IC₅₀ value for nanoparticles in treated 3D mammospheres. 138

Fig. 3.14 *In-vivo* therapeutic evaluation of PEI-Pira/Sal nanoparticles in EAC tumor-bearing mice. (A) Schematic representation of the dosage regimen followed during in-vivo experiments. (B) Relative tumor regression profiles in mice treated with single- and dual-drug-loaded PEI-Pira/Sal nanoparticles compared to saline control. (C) Relative tumor volume comparison on Day 37 post-treatment. Data are expressed as mean \pm SD (n = 3); p > 0.05 indicates no significant difference (ns). 140

Fig. 3.15 Assessment of systemic toxicity and survival in EAC tumor-bearing mice following nanoparticle treatment. (A) Changes in mean body weight of mice over 40 days post-treatment with single and dual-drug-loaded PEI-Pira/Sal nanoparticles compared to saline control. (B) Kaplan–Meier survival analysis of treated versus control groups. Data are presented as mean \pm SD (n = 3); p > 0.05 indicates no significant difference (ns). 141

CHAPTER 4 – Development of Folic Acid-Conjugated Pirarubicin/Salinomycin Dual-Encapsulated PLA-Based Redox-Responsive Block Copolymeric Nanoparticles

Fig. 4.1 Schematic illustration of mechanism of action of FA targeted Pira/Sal co-loaded [S-(PLA-b-PEG-CONH)]₂ nanoparticles on cancer cell 156

Fig. 4.2 Reaction scheme of synthesis of FA-conjugated [S-(PLA-b-PEG-CONH)]₂ block copolymer 169

Fig. 4.3(A) ¹H NMR spectra of [S-(PLA-OH)]₂ 170

Fig. 4.3(B) ¹H NMR spectra of [S-(PLA-COOH)]₂ 170

Fig. 4.3(C) ¹H NMR spectra of [S-(PLA-b-PEG-OH)]₂ 171

Fig. 4.3(D) ¹H NMR spectra of FA-conjugated [S-(PLA-b-PEG-CONH)]₂ block polymer 171

Fig. 4.4 GPC data of FA-conjugated [S-(PLA-b-PEG-CONH)]₂ block copolymer along with all the precursors 172

Fig. 4.5 UV-Visible absorption spectra of Folic acid (FA) and FA-conjugated [S-(PLA-b-PEG-CONH)]₂ polymer recorded in DMF 172

Fig. 4.6 Schematic illustration of preparation of Pira/Sal co-loaded FA- conjugated [S-(PLA-b-PEG-CONH)]₂ redox responsive nanoparticles 174

Fig. 4.7 Comprehensive physicochemical characterization of FA-conjugated [S-(PLA-b-PEG-CONH)]₂ nanoparticles. (A) Hydrodynamic particle size and (B) zeta potential of Pira-loaded, Sal-loaded and dual-loaded nanoparticles as determined by dynamic light scattering (DLS; Anton Paar, Austria). (C) Transmission electron microscopy (TEM; JEOL JEM-1400) images captured at 25,000× magnification with a 200 nm scale bar, confirming uniform spherical morphology. (D) Particle size distribution histograms for (i) Pira-loaded, (ii) Sal-loaded and (iii) dual-loaded nanoparticles, plotted using ImageJ software fitted with a log-normal distribution function. 176

Fig. 4.8 Stability evaluation of FA-conjugated [S-(PLA-b-PEG-CONH)]₂ nanoparticles by DLS-based size analysis at three different temperature conditions; 25 °C, 4 °C and 37 °C 177

Fig. 4.9 Biocompatibility evaluation of FA-conjugated [S-(PLA-b-PEG-CONH)]₂ nanoparticles. (A) Cytocompatibility assessment on NIH 3T3 and HEK 293T cell lines using the MTT assay. (B) Hemocompatibility evaluation through hemolysis (%) analysis. 178

Fig. 4.10 *In-vitro* drug release profiles of Pirarubicin and Salinomycin from single or dual-loaded FA-conjugated [S-(PLA-b-PEG-CONH)]₂ nanoparticles under two conditions: (A) Phosphate buffer solution at physiological pH 7.4 and (B) Reductive environment containing DTT at pH 7.4 180

Fig. 4.11 Cellular internalization of Rhodamine B/Coumarin 6 dual dye-loaded FA-conjugated [S-(PLA-b-PEG-CONH)]₂ nanoparticles in SUM-149 triple-negative breast cancer (TNBC) cells assessed using Confocal Laser Scanning Microscopy (CLSM) in (A) 2D monolayer cultures (B) 3D spheroid models (40X magnification) and (C) Flow cytometry (FACS) analysis based on 10,000 recorded events 181

Fig. 4.12 Non-linear regression curves of *in-vitro* cell proliferation inhibition assay on breast cancer cells

Fig. 4.13 Cytotoxicity analysis of FA-conjugated [S-(PLA-b-PEG-CONH)]₂ nanoparticles in breast cancer cell lines. (A) Sigmoidal dose–response curves showing % cell survival and IC₅₀ values determined by MTT assay. (B) Comparative % cell viability at 1 μM concentration for single and dual-drug-loaded nanoparticles (Pira:Sal ratios of 1:1, 3:1, and 1:3). 184

Fig. 4.14 Cytotoxic evaluation of FA-conjugated [S-(PLA-b-PEG-CONH)]₂ nanoparticles in SUM-149 3D mammospheres. (A) Confocal Laser Scanning Microscopy (CLSM) images of 3D mammospheres before and after treatment with various nanoparticle formulations. (B) Sigmoidal IC₅₀ curve illustrating the cytotoxic response of SUM-149 3D mammospheres to nanoparticle treatment. (C) Comparative analysis of % cell viability at 1 μM concentration for Pira and Sal single-loaded versus dual-loaded nanoparticles (n = 3). 186

Fig. 4.15 Combination index (CI) versus fraction affected (Fa) plots for (A) free Pirarubicin and Salinomycin combinations at varying ratios (Pira:Sal = 1:1, 3:1 and 1:3) and (B) Dual-loaded FA-conjugated [S-(PLA-b-PEG-CONH)]₂ nanoparticles containing Pira and Sal in the same ratios, evaluated against breast cancer cell lines SUM-149, MDA-MB-231 and EAC 187

Fig. 4.16 *In-vivo* antitumor efficacy of FA-conjugated [S-(PLA-b-PEG-CONH)]₂ nanoparticles in EAC tumor-bearing mice. (A) Treatment administration schedule for free drugs and nanoparticle formulations. (B) Relative tumor regression profiles following treatment with free Pira/Sal and single or dual-loaded nanoparticles. (C) Comparative analysis of relative tumor volume on Day 37 post-inoculation. Treatments were continued up to Day 60. 189

Fig. 4.17 Kaplan Meier survival plots of EAC tumor bearing mice treated with free Pira/Sal vs Pira/Sal single or dual-loaded nanoparticles till Day 60 of study and Median survival durations for each treatment group are also summarized 190

Fig. 4.18 Systemic toxicity assessment of free drugs and FA-conjugated [S-(PLA-b-PEG-CONH)]₂ nanoparticles in EAC tumor-bearing mice. (A) Changes in average body weight of mice treated with free

Pira/Sal and Pira/Sal single or dual-loaded nanoparticles throughout the study duration. (B) Histopathological analysis of vital organs using H&E staining in mice treated with free Pira, free Sal, and FA-conjugated Pira/Sal (3:1) dual-loaded nanoparticles. Observations under CLSM at 40× magnification indicated: I-cytoplasmic vacuolization, II-fiber degeneration in cardiac tissue III- abnormal hepatocytes, IV- acute tubular necrosis and V-spleen toxicity

191

LIST OF TABLES

CHAPTER 1 – Introduction and Literature Review

Table. 1.1 Literature survey table summarizing various nanoparticles used as chemotherapy drug delivery carriers that are currently in preclinical or clinical phases	26
--	----

CHAPTER 2 – Development of Pirarubicin/Gemcitabine-Conjugated PLA-Based Block Copolymeric Nanoparticles for Anti-Cancer Efficacy

Table. 2.1 Calculation of Number Average Molecular weight (M_n) and Degree of polymerization (DP) of mPEG-b-PLA via ^1H NMR spectroscopy	82
Table. 2.2 Dynamic Light Scattering (DLS) characterization data	83
Table. 2.3 IC_{50} values of free Pira/Gem vs Pira/Gem-mPEG-b-PLA Nps	95
Table. 2.4 IC_{50} values of free Pira/Gem and their combinations with respect to Pira concentration	97
Table. 2.5 IC_{50} values of Pira/Gem-mPEG-b-PLA-LA single versus dual-loaded nanoparticles	98
Table. 2.6 Combination Index (CI values) of free Pira/Gem drug combinations	99
Table. 2.7 Combination index values of Pira and Gem-mPEG-b-PLA-LA dual-loaded nanoparticles	100

CHAPTER 3 – Development of Pirarubicin/Salinomycin-Polyethyleneimine Conjugates and Their Delivery Using PLA-Based Block Copolymeric Nanoparticles

Table. 3.1 Dynamic Light Scattering data of of single- and dual-loaded PEI-Pira/Sal mPEG-b-PLA nanoparticles	126
---	-----

Table. 3.2 Cumulative drug release percentage of Pira & Sal from single and dual-loaded PEI-Pira/Sal mPEG-b-PLA nanoparticles under different pH conditions 132

Table. 3.3 IC₅₀ values of single and dual-loaded PEI-Pira/Sal mPEG-b-PLA nanoparticles and free drug (Pira/Sal) formulations 134

Table. 3.4 Combination index values (at Fa = 0.5) of PEI-Pira/Sal mPEG-b-PLA dual-loaded nanoparticles (in varying Pira-Sal ratios; 1:1, 3:1 and 1:3) on different breast cancer cell lines 137

CHAPTER 4 – Development of Folic Acid-Conjugated Pirarubicin/Salinomycin Dual-Encapsulated PLA-Based Redox-Responsive Block Copolymeric Nanoparticles

Table. 4.1 Physicochemical characterization of folic acid-conjugated [S-(PLA-b-PEG-CONH)]₂ nanoparticles loaded with Pira, Sal, or both, as determined by dynamic light scattering (DLS): average particle size, zeta potential and polydispersity index (PDI) 174

Table. 4.2 Encapsulation efficiency and drug loading content of Pira and Sal in single and dual drug-loaded nanoparticle formulations 175

Table. 4.3 IC₅₀ values (in μM) of Pira/Sal single and dual-loaded FA-conjugated [S-(PLA-b-PEG-CONH)]₂ nanoparticles on breast cancer cells 182

Table. 4.4 IC₅₀ (μM) values of free Pira/Sal and their combination on breast cancer cells 183

Table. 4.5 Combination Index (CI value) of free Pira/Sal combination or Pira/Sal dual-loaded FA-conjugated [S-(PLA-b-PEG-CONH)]₂ nanoparticles in different ratios (Pira:Sal - 1:1, 3:1 and 1:3) on breast cancer cells at Fa = 0.5 187

GLOSSARY OF SYMBOLS AND ABBREVIATION

g	gram
mg	Milligram
kg	Kilogram
V	Volume
W	Weight
L	Liter
M	Molar
N	Normal
v/v	Volume/Volume
w/v	Weight/volume
m/z	Mass/charge
eV	Electron volt
cm	Centimeter
mm	millimeter
dl	Deciliter
dm	Decimeter
m	Meter
%	Percentage
~	Approximately
μ	micro

\pm	Plus-minus sign
$^{\circ}\text{C}$	Degree centigrade
@	At a rate of
\leq	Less than equals to
\geq	Greater than equals to
λ	Lambda
μg	Microgram
μL	Microliter
μM	Micromolar
nM	Nanomolar
ng	Nanogram
P	Probability
hr	Hour
Hz	Hertz
kDa	Kilodalton
Da	Dalton
mm³	Millimeter cube
mmol	millimolar
mol	molar
min	minutes
rpm	Rotation per minute
Rf	Retention factor
e.g.	For example

i.e.	That is
Et. al	And others
DCM	Dichloromethane
DMF	N,N Dimethyl formamide
DMAP	Dimethyl amino pyridine
Py	Pyridine
R.T.	Room temperature
CHCl₃	Chloroform
MeOH	Methanol
DMSO	Dimethyl sulphoxide
M_n	Number average molecular weight
M_w	Weight average molecular weight
SD	Standard deviation
PSD	Particle size distribution
PLA	Poly lactic acid
LA	Lactic acid
PEG	Polyethylene glycol
mPEG	Methoxy polyethylene glycol
TEM	Transmission electron microscopy
SEM	Scanning electron microscopy
CLSM	Confocal laser scanning microscope
RhoB	Rhodamine B
C6	Coumarin 6

MTT	3-(4,5-dimethylthiazol-2-yl)-2,5-diphenyltetrazolium bromide
DAPI	4',6-diamidino-2-phenylindole
DMEM	Dulbecco's modified eagle medium
RPMI	Roswell park memorial institute
EGF	Epidermal growth factor
bFGF	Basic fibroblast growth factor
DNA	Deoxy ribonucleic acid
DDS	Drug delivery system
FBS	Fetal bovine serum
EAC	Ehrlich ascites carcinoma
EDTA	Ethylene diamine tetra acetic acid
RBC	Red blood cell
WBC	White blood cell
EPR	Enhanced permeability and retention
FDA	Food and drug administration
GPC	Gel permeation chromatography
HPLC	High performance liquid chromatography
FTIR	Fourier transform infrared spectroscopy
NMR	Nuclear magnetic resonance
RALLS	Right angle laser light scattering
LALLS	Low angle laser light scattering
DLS	Dynamic light scattering

H&E	Hematoxylin and Eosin
ANOVA	Analysis of variance
MWCO	Molecular weight cut-off
CSC	Cancer stem cell
IC₅₀	Half maximal inhibitory concentration
Np	nanoparticle
IP	Intraperitoneal
IT	Intratumorally
IV	Intravenous
TNBC	Triple negative breast cancer
pH	Potential of hydrogen
MDR	Multi-drug resistance
EMT	Epithelial to mesenchymal transition
PBS	Phosphate buffered saline